NANO LETTERS

2001
Vol. 1, No. 1
42−44

Precision Attachment of Individual F_1-ATPase Biomolecular Motors on Nanofabricated Substrates

G. D. Bachand,[†] R. K. Soong,[†] H. P. Neves,[†] A. Olkhovets,[‡] H. G. Craighead,[‡] and C. D. Montemagno*,[†]

Nanobiotechnology Center & Department of Agricultural and Biological Engineering and Nanobiotechnology Center & School of Applied and Engineering Physics, Cornell University, Ithaca, New York 14853

Received October 11, 2000

ABSTRACT

The ability to precisely position and orient biological molecules on engineered substrates is an enabling technology critical to the long-term goal of integrating biomolecular motors with nano-electro-mechanical systems. Electron beam lithography and nanoimprinting techniques were used to produce arrays of nickel dots (50–200 nm diameter). Analysis using fluorescence (of microspheres attached to the γ subunit) and atomic force microscopy of these arrays demonstrated precise positioning, spacing, and orientation of individual F_1-ATPase molecules.

Emergent nanofabrication technologies have enabled the production of nanoscale structures and devices with features as small as 7 nm.[1] However, the ability to power such devices has been hindered by the inability to produce silicon-based nanoscale motors with similar size and compatible force generation. Biophysical analysis of a variety of enzymes has revealed that many act as nanoscale biological motors. Enzymes such as kinesin,[2] dynein,[3] myosin,[4] DNA helicase,[5] and RNA polymerase[6] act as linear, stepped motors moving along or shuttling stationary tracks. In contrast, the bacterial flagella protein complex[7] and adenosine triphosphate synthase (ATPase) act as true rotary motors.[8,9] The force generation and size scale of these biomolecular motors are compatible with nanofabricated structures; thus creating the potential exploitation of these enzymes to power hybrid nanoscale devices.[9]

The rotary nature of ATPase was conclusively demonstrated by attaching an actin filament to the γ subunit of a thermostable F_1-ATPase.[8] The γ subunit of F_1-ATPase transitions among three equidistant catalytic sites during hydrolysis.[8] Analysis of these experiments suggests that the work performed by this enzyme exceeds 80 pN·nm and is approximately 100% efficient.[8,10] Similar findings were also reported for an F_1-ATPase from *Escherichia coli* and spinach (*Spinacea oleracea*) chloroplasts.[11] On the basis of its force generation, no-load velocity of ~17 rps[12] and an overall diameter of 10 nm, the F_1-ATPase is a tailor-made molecular motor. Thus, current research being conducted in our laboratory is focused on the integration of F_1-ATPase with nano-electro-mechanical systems (NEMS) to produce a hybrid nanoscale device.[9] Several prerequisite technologies, however, must be established prior to realizing this goal. One fundamental technology centers on the precision attachment of biomolecular motors to engineered, nanofabricated substrates. The future evolution of the underlying mechanisms for interfacing biological molecules with NEMS will provide the impetus for further development of advanced hybrid devices.

Two methods, electron beam (e-beam) and nanoimprint lithography, were used to create nanofabricated substrates capable of precisely and accurately positioning individual biological motors. In the first method, a standard silicon wafer was coated with two layers of electron beam-sensitive polymer poly(methyl methacrylate) (PMMA) resist, with the lower layer being slightly more sensitive to the e-beam exposure. Arrays were patterned into the bilayer using e-beam lithography, followed by development. A 5 nm tantalum (Ta) adhesion layer and a 10 nm metallic nickel (Ni^{2+}) layer were deposited using electron-beam physical vapor deposition. Lift-off was performed using a 1:1 solution of methylene chloride:acetone for 15 min followed by ultrasonic agitation for 10 s. Regular arrays of 60−600 nm size dots on 1 μm pitch with circular profiles were confirmed by scanning electron microscopy. Arrays were stored under appropriate conditions (e.g., vacuum) to prevent oxidation of the Ni surface prior to experimental use.

* Corresponding author. E-mail: cdm11@cornell.edu.
[†] Nanobiotechnology Center & Department of Agricultural and Biological Engineering.
[‡] Nanobiotechnology Center & School of Applied and Engineering Physics.

10.1021/nl005513i CCC: $20.00
Published on Web 12/21/2000

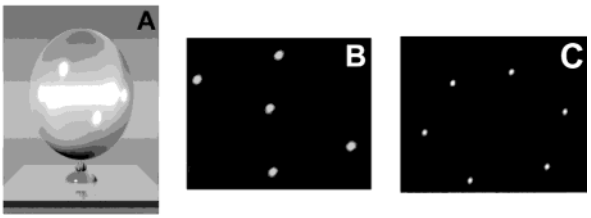

Figure 1. Schematic diagram (A) and CCD photomicrograph (B) of fluorescent microspheres attached to the γ subunit of individual F_1-ATPase molecules immobilized on nickel dot arrays that were created using electron beam lithography.

The precision attachment of individual F_1-ATPase biomolecular motors on the Ni dot arrays was demonstrated using two methods. In the first method, a recombinant F_1-ATPase from the thermophilic bacterium, Bacillus PS3 was expressed in pKK223-3 (Amersham Pharmacia Biotech, Piscataway, NJ) and purified using ion exchange and size exclusion chromatography.[9] The recombinant F_1-ATPase was specifically engineered for integration with nanomechanical systems and contained a 10x Histidine (His) tag on each of the β subunits, as well as a unique cysteine residue at the tip of the γ subunit (γCys). The His tags were engineered onto the β subunits due to the high affinity of poly-His for cationic Ni conjugated to a variety of media, as well as metallic Ni.[13] F_1-ATPase molecules were specifically biotinylated through disulfide linkage between γCys and biotin malemide in the presence of *N*′,*N*′-dimethylformamide. Biotinylated F_1-ATPase molecules (100 μg/mL in 10 mM phosphate buffer, pH 7.0) were allowed to attach to Ni arrays through diffusion and adhesion to dots for 15 min at room temperature, followed by washing with phosphate buffer. Subsequently, 1 μm streptavidin-coated, fluorescent microspheres were incubated on the arrays, followed by washing with phosphate buffer to remove all unbound microspheres. A schematic diagram of the F_1-ATPase-microsphere complex is presented in Figure 1A. As a control, arrays also were incubated with streptavidin-coated microsphere in the absence of F_1-ATPase.

Attachment of F_1-ATPase-microsphere complexes was examined using epifluorescence microscopy, demonstrating attachment of the complexes in specific array patterns (Figure 1B,C). F_1-ATPase molecules did not attach to all dots in the array; however, at least 50% attachment was observed over large areas. Streptavidin-coated microspheres were not observed on arrays that had not been coated with F_1-ATPase. Oxidation of Ni dots potentially may have limited the number of chemically active dots capable of binding F_1-ATPase motors. Other factors such as diffusion rates and F_1-ATPase concentration may be important in regulating the efficacy of attachment. In order for adhesion to occur, the F_1-ATPase must attach to the Ni surface through the His-tags engineered on the β subunit of the molecule, thus leaving the biotinylated γ subunit perpendicular to the substrate and able to bind a streptavidin-coated microsphere. Because the γ subunit of F_1-ATPase rotates in response to ATP hydrolysis, the molecule is correctly oriented to utilize the rotary nature of the γ subunit. Overall, this experiment demonstrates the ability to precisely position F_1-ATPase motors in two dimensions (i.e., *x* and *y*), with the proper orientation for utilizing the work performed by the γ subunit during ATP hydrolysis.

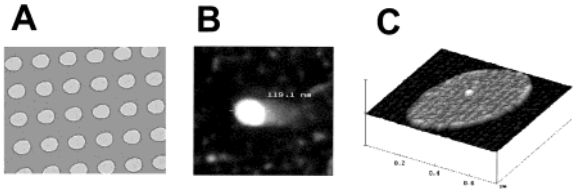

Figure 2. Nickel dots array fabricated using electron beam lithography (A, B), and used to attach of single F_1-ATPase molecules (C). Dots were 60−600 nm diameter and 4−20 nm high.

Because the previous experiment could not eliminate the potential adhesion of more than one F_1-ATPase molecule per dot, atomic force microscopy (AFM) was used to verify the precise attachment of individual biological molecules on nanofabricated arrays. Biotinylated F_1-ATPase molecules (10−1000 μg/mL in 10 mM phosphate buffer, pH 7.0) were allowed to attach to Ni arrays, as described above, for 15 min at room temperature. Following extensive washing with phosphate buffer, arrays were imaged in tapping mode AFM (Dimension 3000 scanning probe microscope, Digital Instruments, Santa Barbara, CA) to reduce the force between the tip and the sample. Arrays prior to addition of F_1-ATPase, as well as arrays coated with phosphate buffer, were used as negative controls.

AFM imaging of nickel dot (60−600 nm diameter, 4−20 nm high) arrays produced by e-beam lithography demonstrated the presence of individual F_1-ATPase molecules (14 nm high and 8 nm diameter) on the nickel dots (Figure 2). The apparent diameter of the F_1-ATPase molecules was 30−50 nm due to AFM tip−F_1-ATPase convolution. Deflection in the AFM tips corresponding to the presence of F_1-ATPase motors was easily observed due to the relatively smooth surface of the dots. Nickel arrays incubated with 10 mM phosphate buffer (pH 7.0) were used as controls; no protrusions were observed (Figure 2), substantiating the identity of F_1-ATPase with the AFM. Depending upon F_1-ATPase concentration and Ni dot size, the density of F_1-ATPase varied from one molecule per 30 dots to 2−3 molecules per dot. In general, smaller dot sizes preclude the adhesion of more than one F_1-ATPase molecule per dot.

Despite the ability to generate nanoscale, biocompatible substrates, e-beam lithography is intrinsically slow and thus limits the size and number of arrays that can be produced at one time. Optical lithography, on the other hand, cannot produce such small dimensions due to the wavelengths employed. An alternative strategy, nanoimprint lithography,[14] has been used to obtain large numbers of nanoscale structures including nanometer-size dots. Consequently, this process is well suited for producing large nickel dot arrays for precision attachment of biological molecules. The enhanced production capabilities associated with nanoimprint is appropriate for the subsequent application of these arrays for constructing integrated nanomechanical devices powered by biomolecular motors.

Nanoimprint lithography involves transferring engineered patterns from a mold by physically pressing it against a surface previously coated with a polymer (e.g., PMMA). In

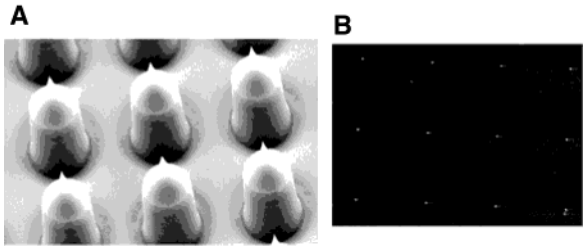

Figure 3. Optical lithography was used to create the nanoimprinting mold (A), which subsequently was used to create large arrays of nickel dots (B). Dots were 50−250 nm diameter and 5−15 nm high.

this case, the mold consisted of atomically sharp tips and was fabricated on a monocrystalline silicon substrate. Dots, 500 nm in diameter, were defined by photolithography using an i-line stepper. The pattern was transferred onto the silicon dioxide layer through fluorine- and chlorine-based reactive ion etching (RIE), followed by thermal oxidization of the silicon for initial definition of the tip structure. Because of a stress effect around the neck of the post,[15] a nanometer-scale, sharp tip was obtained (Figure 3). RIE was used again to remove the oxide from the floor of the structure, followed by chlorine-based RIE to further etch the silicon and create a shaft for the tips. The oxide was removed using a 1:6 buffered hydrofluoric acid solution.

To form the patterned arrays, the mold was pressed against a quartz substrate or silicon wafer coated with PMMA and heated to 120 °C (above the glass transition temperature of PMMA). A mold release agent (e.g., a 10% solution of lanolin in mineral oil) was used to facilitate the withdrawal of the mold. The tips only penetrated partially into the PMMA to prevent damage to the structure. An oxygen-based RIE was therefore used to extend the printed pattern down to the surface of the substrate to form the base of the dots. Finally a metal film (i.e., Ni) was deposited and then lifted off to expose the nickel arrays (Figure 3).

Arrays produced using nanoimprint lithography contained uniform nickel dots of 50−250 nm diameter. Arrays were missing a small percentage of dots depending upon the variables in imprinting. Larger arrays (10−20 times larger) could be produced with nanoimprint, as compared to e-beam lithography. Attachment of F_1-ATPase biomolecular motors was confirmed using fluorescence microscopy as described above; similar patterns and efficiency of F_1-ATPase attachment to Ni arrays were observed. Hence, nanoimprint lithography offers a viable alternative for production of biocompatible arrays capable of precisely attaching biomolecular motors.

Both nanofabrication methodologies, nanoimprint and e-beam lithography, were capable of producing nanoscale, biocompatible arrays for specifically attaching biomolecular motors. The ability to precisely position and orient individual biological molecules represents an enabling technology fundamental to creating hybrid NEMS devices powered by biomolecular motors.[9] The processes and chemistries outlined above have established a system for integrating organic and inorganic materials in an engineered system. Further refinement of the processes will permit the construction of Ni arrays with objective and design specific patterns. In addition, NEMS structures such as valves and pumps can be integrated into this system and permit the construction of novel, useful nanomechanical devices powered by biomolecular motors.

Acknowledgment. We thank Marlene Bachand, Scott Stelick, and Jeremy Ho for providing the technical support for laboratory equipment and experimental tests. We also thank Francis Peters for his support with graphics. This work was sponsored by the Defense Advanced Research Projects Agency, Office of Naval Research, National Science Foundation, National Aeronautics & Space Administration and Department of Energy.

References

(1) (a) Sone, J.; Fujita, J.; Ochiai, Y.; Manako, S.; Matsui, S.; Nomura, E.; Baba, T.; Kawaura, H.; Sakamoto, T.; Chen, C. D.; Nakamura, Y.; Tsai, J. S. *Nanotechnology* **1999**, *10*, 135−141. (b) Block, S. M. *Cell* **1998**, *93*, 5−8.
(2) Schnitzer, M. J.; Block, S. M. *Nature* **1997**, *388*, 386−390.
(3) Mazumdar, M.; Mikami, A.; Gee, M. A.; Vallee, R. B. *Proc. Natl. Acad. Sci. U.S.A.* **1996**, *93*, 6522−6556.
(4) Kitamura, K.; Tokunaga, M.; Iwane, A. H.; Yanagida, T. A. *Nature* **1999**, *397*, 129−134.
(5) Lohman, T.; Thorn, K.; Vale, R. D. *Cell* **1998**, *93*, 9−12.
(6) Wang, M.; Schnitzer, M.; Yin, H.; Landick, R.; Gelles, J.; Block, S. *Science* **1998**, *282*, 902−907.
(7) (a) Berry, R.; Berg, H. *Proc. Natl. Acad. Sci. U.S.A.* **1997**, *94*, 14433−14437. (b) DeRosier, D. *Cell* **1998**, *93*, 17−20.
(8) (a) Noji, H.; Yasuda, R.; Yoshida, M.; Kinosita, K., Jr. *Nature* **1997**, *386*, 299−302. (b) Yashuda, R.; Noji, H.; Kinosita, K., Jr.; Yoshida, M. *Cell* **1998**, *93*, 1117−1124.
(9) Montemagno, C. D.; Bachand, G. D. *Nanotechnology* **1999**, *10*, 225−231. (b) Bachand, G. D.; Montemagno, C. D. *Biomedical Microdevices* **2000**, *2*, 179−184. (c) Soong, R. K.; Bachand, G. D.; Neves, H. P.; Olkhovets, A. G.; Craighead, H. G.; Montemagno, C. D. *Science* **2000**, *290*, 1555−1558.
(10) (a) Kinosita, K., Jr.; Yasuda, R.; Noji, H.; Adachi, K. Philos. *Trans. R. Soc. London Ser. B−Biol. Sci.* **2000**, *355*, 473−489. (b) Kinosita, Jr., K. *Faseb J.* **2000**, *14*, 1567.
(11) (a) Omote, H.; Sambonmatsu, N.; Saito, K.; Sambongi, Y.; Iwamoto-Kihara, A.; Yanagida, T.; Wada, Y.; Futai, M. *Proc. Natl. Acad. Sci. U.S.A.* **1999**, *96*, 7780−7784. (b) Hisabori, T.; Kondoh, A.; Yoshida, M. *FEBS Lett.* **1999**, *463*, 35−38.
(12) Sabbert, D.; Engelbrecht, S.; Junge, W. *Nature* **1996**, *381*, 623−625.
(13) (a) Barklis, E.; McDermott, J.; Wilkens, S.; Fuller, S.; Thompson, D. *J. Biol. Chem.* **1998**, *273*, 7177−7180. (b) Lanfermeijer, F. C.; Venema, K.; Palmgreen, M. G. *Protein Express. Purif.* **1998**, *12*, 29−37. (c) Soong, R. K.; Stelick, S. J.; Bachand, G. D.; Montemagno, C. D. Technical Proceedings of the Second International Conference on Modeling and Simulation of Microsystems, San Juan, Puerto Rico, April 19−21, 1999; pp 95−98.
(14) (a) Chou, S. Y.; Krauss, P. R.; Renstrom, P. J *J. Vac. Sci. Technol. B* **1996**, *14*, 4129−4133. (b) Chou, S. Y.; Krauss, P. R.; Zhang, W.; Guo, L. J.; Zhuang, L. *J. Vac. Sci. Technol. B* **1997**, *15*, 2897−2904. (c) Li, M. T.; Wang, J. A.; Zhuang, L.; Chou, S. Y. *Appl. Phys. Lett.* **2000**, 76, 673−675.
(15) Marcus, R. B.; Ravi, T. S.; Gmitter, T. *Appl. Phys. Lett.* **1990**, *56*, 236−238.

NL005513I